Research Article

Hui Lu*, Dongchuan Xu, Liqiang Zhao, Hailing Ruan, Anguo Wang, Yejuan Li and Weiying Lu*

Promotion of asthenozoospermia by C9orf72 through suppression of spermatogonia activity via fructose metabolism and mitophagy

https://doi.org/10.1515/med-2025-1344
Received August 1, 2025; accepted October 23, 2025;
published online December 30, 2025

Abstract

Objectives: To investigate the involvement of C9orf72 in asthenozoospermia and its effects on spermatogonial energy metabolism and mitophagy.

Methods: Semen samples from 24 asthenozoospermic patients and 28 healthy controls were analyzed for C9orf72 expression and sperm motility. GC-1 spg cells were transduced with C9orf72-overexpressing lentivirus to evaluate changes in energy metabolism, mitophagy, and proliferation. Protein docking and site-directed mutagenesis were used to validate C9orf72-LC3 interactions.

Results: C9orf72 was upregulated in asthenozoospermic samples and negatively correlated with progressive motility. In GC-1 cells, overexpression led to fructose accumulation, reduced glycolytic enzymes, elevated NADH/NAD^+ ratio, suppressed proliferation, and increased oxidative stress. Mitophagy was suppressed, with diminished LC3 fluorescence and reduced autophagosome–mitochondria colocalization. Molecular docking and co-immunoprecipitation confirmed direct C9orf72–LC3 binding, and site-directed mutagenesis identified His128 of C9orf72 as a critical residue for this interaction. LC3 overexpression partially rescued the metabolic and mitophagic defects.

Conclusions: C9orf72 overexpression may contribute to sperm dysfunction in asthenozoospermia by disrupting metabolic homeostasis and mitophagy. These findings provide a new perspective for studying the molecular mechanisms of asthenozoospermia, while the potential of C9orf72 as a diagnostic or therapeutic target requires further verification.

Keywords: C9orf72; asthenozoospermia; sperm progressive motility; fructose metabolism; mitophagy; spermatogonia

Introduction

Asthenozoospermia, defined by reduced sperm motility, accounts for approximately 20 % of male infertility cases worldwide [1]. According to the World Health Organization (WHO) 2010 criteria, it is diagnosed when progressive motility is below 32 % or total motility is under 40 %, with other semen parameters remaining within normal ranges [2]. The incidence of asthenozoospermia has been increasing, potentially due to environmental pollution, occupational stress, and sexually transmitted diseases [3]. Mitochondrial dysfunction and altered energy metabolism contribute to impaired sperm motility, but 30–40 % of cases remain unexplained [4, 5]. Current treatment options include pharmacological therapies (e.g., phosphodiesterase inhibitors) and *in vitro* fertilization [6, 7]. However, their application is limited by side effects, high costs, and technical barriers, leading many infertile couples to rely on assisted reproductive technologies, which are costly and may cause complications such as salpingitis and endometriosis [8]. Investigating the regulation of sperm mitochondrial function and energy mechanisms may provide new therapeutic targets for asthenozoospermia [9, 10].

Mitochondria form a helical sheath in the sperm midpiece, serving as the primary site of energy metabolism. Oxidative phosphorylation (OXPHOS) supports sperm motility, the acrosome reaction, and hyperactivation, and also regulates calcium signaling and redox homeostasis [4]. Efficient OXPHOS, particularly through electron transport chain complex II (CII), enhances sperm metabolic function, motility, and fertilizing capacity [11]. Autophagy is essential for maintaining mitochondrial function, and reduced expression of autophagy-related genes in men with poor sperm quality suggests a role in

***Corresponding authors: Hui Lu and Weiying Lu**, Reproductive Medical Center, Hainan Women and Children's Medical Center, No.75 Longkun South Road, Haikou, 570206, Hainan, China, E-mail: waluhui@muhn.edu.cn (H. Lu), Luweiying206@163.com (W. Lu). https://orcid.org/0009-0000-3178-9882 (H. Lu)

Dongchuan Xu, Department of Emergency Medicine, Hainan Affiliated Hospital of Hainan Medical University, Hainan General Hospital, Haikou, Hainan, China

Liqiang Zhao, **Hailing Ruan**, **Anguo Wang and Yejuan Li**, Reproductive Medical Center, Hainan Women and Children's Medical Center, Haikou, Hainan, China

asthenozoospermia [12]. Impaired mitophagy results in the accumulation of dysfunctional mitochondria, leading to increased reactive oxygen species (ROS), loss of membrane potential, reduced OXPHOS efficiency, and diminished ATP production [13]. Interventions that activate autophagy pathways, such as enhancing BNIP3/LC3 function or restoring PINK1/Parkin signaling, have been shown to improve mitochondrial quality and sperm motility [14, 15].

Our previous work demonstrated elevated C9orf72 (NM_028466.2) expression in seminal exosomes from asthenozoospermic patients, suggesting a potential role in disease pathogenesis [16]. C9orf72 functions as a guanine nucleotide exchange factor [17, 18] and has been shown to regulate autophagy initiation through interaction with the Rab1a-ULK1 complex [19]. The C9orf72–SMCR8 complex further modulates ULK1/ATG1 kinase activity to promote autophagy [20]. Although these autophagy-related functions are established, the role of C9orf72 in mitophagy regulation remains unclear. Recent evidence indicates that C9orf72 localizes to the mitochondrial membrane, where it stabilizes complex I and contributes to energy balance [21]. In addition, C9orf72 may interfere with mitochondrial trafficking to metabolically active sites [22].

Fructose, secreted predominantly by the seminal vesicles, is a critical energy substrate for sperm. Several studies have reported an inverse association between seminal fructose levels and progressive motility [23, 24], although the mechanisms remain unclear. Given that mitophagy impairment contributes to defective sperm function, it remains unclear whether C9orf72 regulates this pathway in the context of asthenozoospermia. It is yet to be determined whether C9orf72 promotes asthenozoospermia by inhibiting mitophagy and fructose metabolism. GC-1 spermatogonia (spg) cells, an immortalized mouse line, are widely used to model spermatogenic function and stress responses, including glucose-induced apoptosis, oxidative stress, and autophagy [25, 26]. This study examines C9orf72 expression in asthenozoospermia patients and explores its impact on GC-1 spg cell proliferation, focusing on potential regulatory roles through mitophagy and fructose metabolism. These insights may pave the way for identifying novel molecular targets in the treatment of male infertility associated with impaired sperm motility.

Materials and methods

Study participants

Human semen samples were collected from Hainan Provincial Maternal and Child Health Hospital following ethical approval (No. 2021–033) from the Ethics Committee of Hainan Women and Children's Medical Center. All experimental procedures involving human participants were conducted in accordance with the ethical principles outlined in the Declaration of Helsinki. Prior to inclusion in the study, each participant provided written informed consent. Sample size estimation was performed based on established statistical principles [27, 28]. Assuming α=0.05, power=0.80, a clinically meaningful difference (δ) of 5 %, and an expected standard deviation (σ) of 10 %. Participants with abnormal semen biochemical markers (e.g., fructose, acid phosphatase, α-glucosidase), atypical physical properties (e.g., liquefaction time, pH), or abnormal sperm morphology were excluded. The asthenozoospermia group (n=24) met the following criteria: (1) progressive motility <32 % or total motility <40 %; (2) sex hormone levels within the normal physiological range; (3) no detectable abnormalities observed during physical examination of the reproductive system; (4) total sperm count ≥39 million per ejaculate and >4 % morphologically normal sperm, based on WHO 2010 standards [2]. The control group (n=28) included men with progressive motility ≥32 % or total motility ≥40 %, while meeting all other inclusion criteria identical to those of the asthenozoospermia group.

Semen analysis

Semen analysis was performed following the guidelines set by the WHO in the Laboratory Manual for Human Semen Examination and Processing (5th edition, 2010) [29]. Semen samples were liquefied at 37 °C for 30 min, then the samples were mixed by pipetting to ensure uniformity. A suitable volume of the liquefied semen sample was then loaded into a pre-warmed counting chamber compatible with the Sperm Quality Analyzer (SCA, Microptic S.L., Barcelona, Spain). The system is capable of accurately measuring sperm concentration (10^6/mL) and evaluating sperm progressive motility, non-progressive motility, and immotile sperm.

Immunofluorescence

Semen specimens were collected into sterile containers and subsequently diluted with PBS (phosphate-buffered saline, pH 7.4, Sigma-Aldrich, USA) in flat-bottom centrifuge tubes. After gentle mixing, samples were centrifuged at 1,000×*g* for 15 min. The supernatant was removed, and the cell pellet was fixed in 4 % buffered paraformaldehyde (in PBS, pH 7.4) for 30 min at room temperature. Fixed samples were evenly smeared onto microscope slides, followed by air-drying at room temperature. For sperm samples, immunofluorescence staining was performed using an anti-C9orf72 primary antibody (ab308169, Abcam, 1:250), followed by incubation with a fluorescent secondary antibody (anti-rabbit A0516, Beyotime,

1:250). Nuclei were counterstained with DAPI (Sigma-Aldrich, D9542). The mean fluorescence intensity (MFI) of C9orf72 staining was quantified from regions of interest (ROIs) using ImageJ software (version 1.8.0, NIH) after background subtraction. Smears of GC-1 spg cells were prepared using the same procedure. Following air drying, slides were rinsed with PBS and blocked with goat serum (Beyotime, C0265) for 2 h. Primary antibodies against C9orf72 (ab308169), LC3 (ab192890), and TOM20 (ab56783) were purchased from Abcam and used at a dilution ratio of 1:250. Following overnight incubation at 4 °C, samples were washed thoroughly with PBS. Fluorescent secondary antibodies (anti-rabbit A0516 and anti-mouse A0521, both from Beyotime, 1:250 dilution) were then applied for 1 h at room temperature. Nuclei were counterstained using DAPI (Sigma-Aldrich, D9542), and fluorescent signals were subsequently visualized using a Leica TCS SP2 confocal laser scanning microscope. Colocalization of LC3-labeled autophagosomes with TOM20-labeled mitochondria was evaluated by confocal microscopy as previously described [30]. Colocalization between LC3 and TOM20 was quantified using Pearson's correlation coefficient (r) as described by Jeremy et al. [31]. Briefly, the analysis was performed on maximum projection images of individual cells. Calculations were carried out using the Just Another Colocalisation Plugin (JACoP) in ImageJ (version 1.8.0).

Western blot

Liquefied semen samples were centrifuged at 500×*g* for 10 min to isolate sperm cells, which were then washed with cold PBS and resuspended for protein extraction. Lysis was performed using RIPA buffer (Thermo Fisher Scientific, 89,900) on ice for 30 min, followed by centrifugation at 12,000×*g* for 15 min at 4 °C. Protein concentration was measured using a BCA assay (Thermo Fisher Scientific, 23,225). Equal amounts of protein (50 μg) were separated by 10 % SDS-PAGE (Bio-Rad, 1610184) and transferred to PVDF membranes (Millipore, IPVH00010). The membrane was incubated overnight at 4 °C with primary antibodies listed in Table S1. HRP-conjugated secondary antibodies were applied for detection. The protein bands were detected and imaged using ECL reagents (Thermo Fisher, 32,106). GAPDH expression was used as a loading control to normalize relative protein expression, and ImageJ software (NIH, V1.8.0.112) was used for analysis.

Cell culture, lentivirus construction and transduction

A mouse spermatogonia cell line (GC-1 spg cells) (Procell Life Science and Technology, CL-0600) was cultured in GC-1 spg cell complete medium (Procell Life Science and Technology, CM-0600) containing DMEM supplemented with 10 % fetal bovine serum and 1 % penicillin-streptomycin, in a humidified incubator at 37 °C with 5 % CO_2. GC-1 spg cells serve as a well-established *in vitro* model for studying spermatogonial cell function and spermatogenesis-related molecular pathways relevant to male infertility [32, 33]. Mouse coding sequence of C9orf72 was obtained from National Center for Biotechnology Information database. Using synthesized full-length coding sequence (NM_028466.2), we constructed recombinant lentivirus by cloning into GV358 vector (Genewiz, China). For virus production, 293T cells were co-transfected with the expression vector, viral envelope plasmid, packaging plasmids using Lipofectamine 3,000 (Invitrogen, L3000015). After 48 h incubation, viral particles were harvested from supernatant through concentration and purification steps. GC-1 spg cells were transduced with lentivirus at a multiplicity of infection (MOI) of 20 in the presence of poly-L-lysine (Gene Chem), and subjected to further experiments 96 h post-transduction. The culture medium was refreshed 12 h after infection, and all groups were maintained under identical conditions. To exclude the possibility that viral infection itself caused cytotoxicity, two control groups were included: a blank control group (CON, no viral treatment) and a negative control group (NC, lentivirus carrying an empty GV358 vector under the same conditions as the experimental group). Transduction efficiency was preliminarily assessed by qPCR and Western blot.

RT-PCR

Total RNA from GC-1 spg cells was isolated using TRIzol reagent. All procedures employed RNase-free consumables and Takara RT-PCR kit (RR036A). Expression levels of C9orf72 were quantified by SYBR Green-based qPCR, with GAPDH serving as the internal reference gene for normalization. Reactions were run on an Agilent Stratagene Mx3000P system. The relative gene expression was calculated using the $2^{-\Delta\Delta Ct}$ method, with each sample assayed in triplicate. The PCR cycling protocol was: initial denaturation at 95 °C for 2 min, denaturation at 94 °C for 20 s, annealing at 58 °C for 20 s, extension at 72 °C for 20 s, repeated for 40 cycles. Melting curve analysis was performed with the following steps: 94 °C for 30 s, 65 °C for 30 s, and a final step at 94 °C for 30 s. Primer sequences were listed in Table S2.

Cell viability assay

To evaluate the proliferative activity of GC-1 spg cells over time, approximately 5×10^3 cells per well were carefully plated into 96-well flat-bottom microplates and allowed to adhere overnight under standard culture conditions. CCK-8 reagent (CK04) was purchased from Dojindo. The next day, each well received 10 μL of CCK-8 reagent, followed by continuous incubation for 6 h to enable full color development. Absorbance at 450 nm was recorded using a UV-1900 spectrophotometer (Shimadzu, Japan). This procedure was repeated daily over five consecutive days, with three parallel wells per time point to ensure data consistency. Results were interpreted based on OD_{450} shifts as a surrogate for cell viability.

Flow cytometry analysis

After digestion, logarithmic phase GC-1 spg cells were resuspended in PBS, then subjected to Annexin V-FITC/propidium iodide dual staining (BD Biosciences, 556547). Cellular apoptosis was assessed utilizing a FACSAria flow cytometer (Becton Dickinson, USA).

ROS detection

To assess oxidative stress status, GC-1 spg cells were first standardized to 1×10^6 cells/mL in complete medium. The ROS-sensitive probe DCFH-DA (Beyotime, S0033) was employed at a working concentration of 10 μM. Cell suspensions were incubated in the dark at 37 °C with 5 % CO_2 for 20 min, during which gentle pipette mixing was performed every 5 min to maintain homogeneous probe exposure. Post-incubation, cells underwent two washes in cold PBS (pH 7.4) to eliminate residual dye. The cleaned suspension was diluted in chilled PBS to 10 mL, centrifuged at 300×*g* for 5 min, and the resulting pellet was resuspended in 1 mL PBS. Fluorescence intensity, corresponding to intracellular ROS levels, was acquired on a FACSAria cytometer, using excitation at 488 nm and emission detection at 530 nm.

ELISA

The supernatant of each group of GC-1 spg cells was collected, and 200 μL of sample was used for ELISA detection of fructose concentration by fructose assay kit (Abcam, ab83380). The samples were diluted 1:5, and the absorbance at 450 nm was measured to generate a standard curve for concentration calculation. Background absorbance correction was applied to minimize interference from other metabolites in this optical range. GAPDH enzymatic activity was determined using GAPDH ELISA Kit (Abcam, ab176642) in GC-1 spg cells. A total of 1×10^6 cells were lysed, and the assay was performed. Absorbance at 450 nm was measured to calculate GAPDH enzyme activity. The intracellular NADH/NAD^+ ratio (nicotinamide adenine dinucleotide, reduced/oxidized form) was evaluated using a NAD/NADH assay kit (Colorimetric) (Abcam, ab65348).

Seahorse XF analysis

Cellular oxygen consumption was assessed with an XF analyzer (Agilent Technologies, Santa Clara, CA) according to previously published methodology [34]. 2×10^4 cells per well C9orf72 overexpression and empty vector control GC-1 spg cells were seeded in Seahorse XF-specific microplates. Cells were maintained in bicarbonate-free DMEM with 1 h equilibration at 37 °C before measurement. Sequential injections were performed during the assay: oligomycin (1 μM, ~16 min) to inhibit ATP synthase and thereby quantify ATP-linked respiration, FCCP (1.5 μM, ~40 min) as a mitochondrial uncoupler to collapse the proton gradient and reveal maximal respiratory capacity, and rotenone/antimycin A (1 μM each, ~60 min) to inhibit complexes I and III, respectively, thereby blocking mitochondrial electron transport and enabling assessment of non-mitochondrial respiration. OCR parameters including basal respiration, ATP-linked respiration, maximal respiration, and spare respiratory capacity were calculated according to the manufacturer's protocol. For quantification, OCR values were normalized to total protein content in each well (measured by BCA assay after the run), and bar graphs summarizing basal and maximal respiration were generated from three independent experiments.

Protein molecular docking analysis

The protein interaction interface between C9orf72 and LC3 was predicted using the SwissDock online server. LC3 (PDB ID: 4ZBJ) and C9orf72 (AlphaFold predicted structure) were downloaded from the Protein Data Bank and analyzed using AutoDock software for molecular docking. Grid parameters were set to cover the LC3 structure surface, and the Lamarckian genetic algorithm was used for molecular docking. The lowest binding energy complex was calculated, and PyMOL software was used for visualization. Key residues potentially influencing LC3 binding were identified, and the

top 10 conformations with the lowest binding free energy were statistically analyzed, followed by hydrogen bond and hydrophobic interaction analysis.

Co-immunoprecipitation

Co-immunoprecipitation was performed to detect the interaction between C9orf72 and LC3. GC-1 spg cells were transduced with lentivirus expressing C9orf72 with a 3 × Flag tag, and cell lysates were collected as input samples, and the lysates were incubated with LC3 antibody (Abcam, ab229327, 1:100) for the first round of immunoprecipitation. Following washing, the immunoprecipitates were analyzed by Western blot using anti-C9orf72 and anti-LC3 antibodies (The same as the Western blot section, listed in Table S1). For the second Co-IP, Flag-tagged wild-type and mutant C9orf72 constructs (H65A, H128A, K83A, and K422A; mutation design in Supplementary File 1) were subjected to immunoprecipitation using Flag antibody (Sigma-Aldrich, F7425, 1:100). The eluted protein complexes were analyzed by Western blot with anti-LC3 and anti-C9orf72 antibodies. IgG controls were included to account for non-specific binding. All experiments were independently repeated three times, and band intensities were quantified using ImageJ software.

Statistical analysis

All statistical analyses were conducted using GraphPad Prism (version 9.0, GraphPad Software, USA). Quantitative data are expressed as the mean±standard deviation (SD). Non-parametric data are presented as the median (interquartile range, IQR). Differences between two groups were analyzed using the unpaired Student's t-test for normally distributed data and the Mann–Whitney U test for non-parametric data. For comparisons among more than two groups, one-way ANOVA was used, while comparisons involving multiple factors were assessed through two-way ANOVA. Correlations between variables were evaluated using Pearson correlation analysis. $p<0.05$ was regarded as indicative of statistical significance.

Ethical approval

All experimental procedures involving human participants were reviewed and approved by the Ethics Committee of Hainan Women and Children's Medical Center (No. 2021–033), and were conducted in accordance with institutional guidelines. Written informed consent was obtained from each participant prior to sample collection. The study adhered to the ethical standards outlined in the 1964 Declaration of Helsinki and its subsequent revisions, ensuring the protection of participants' rights and privacy.

Results

Elevated C9orf72 expression in asthenozoospermia semen and its inverse correlation with sperm progressive motility

A total of 52 semen samples were analyzed, including 24 from individuals diagnosed with asthenozoospermia and 28 from healthy male controls. The corresponding clinical characteristics are summarized in Table 1. Immunofluorescence staining demonstrated markedly increased C9orf72 expression in sperm from asthenozoospermic patients compared to controls, with signals observed in both the head and tail regions (the latter often presenting as a linear green fluorescence along the tail in asthenozoospermia samples). Quantitative analysis of mean fluorescence intensity confirmed significantly higher C9orf72 expression in the asthenozoospermia group than in controls ($p<0.001$; Figure 1A). Western blot showed significant upregulation of C9orf72 protein expression in the asthenozoospermia group compared to the normal group ($p<0.001$) (Figure 1B). Further statistical evaluation revealed a strong inverse correlation between C9orf72 protein expression and sperm progressive motility ($r=-0.8436$, $p<0.001$; Figure 1C). In addition to the highly significant differences observed in total motility, progressive motility, and immotility, non-progressive motility was also statistically different between the two groups ($p=0.028$), as shown in Table 1. These results suggest that elevated C9orf72 expression is associated with reduced sperm motility.

C9orf72 overexpression is associated with reduced proliferation of GC-1 spg cells

GC-1 spg mouse spermatogonial cells were transduced with C9orf72 overexpression lentivirus or negative control virus (NC). RT-PCR was employed to determine the mRNA expression levels of C9orf72, and Western blot was performed to evaluate C9orf72 protein expression. The CCK-8 assay assessed changes in cell viability, and flow cytometry was used to detect apoptosis and ROS levels. Compared to the NC group, the C9orf72 overexpression lentivirus transduction group exhibited a significant increase in both C9orf72 mRNA expression ($p<0.001$)

Table 1: Clinical data of normal and asthenozoospermic semen samples.

Parameter	Normal (n=28)	Asthenozoospermic (n=24)	p-Value
Age, years	33 (30, 35)	33 (32, 38)	0.777
Body mass index, BMI	22.28 ± 1.42	21.99 ± 1.80	0.650
Days of abstinence	3 (3, 4)	4 (3, 6)	0.161
Ejaculate volume, mL	3.06 ± 0.92	3.79 ± 1.52	0.449
Sperm concentration, 10^6/mL	76.26 ± 38.03	58.87 ± 47.34	0.312
Total sperm count, 10^6	216.75 ± 83.456	162.03 ± 107.71	0.161
Total motility, %	53.58 ± 8.41	16.80 ± 11.29	<0.0001
Non-progressive motility (NP), %	8.46 ± 2.50	5.69 ± 3.47	0.028
Progressive motility (PR), %	47.69 ± 8.74	12.00 ± 9.87	<0.0001
Immotile sperm rate, %	43.84 ± 10.14	83.23 ± 12.45	<0.0001
pH	7.2 (7.2, 7.2)	7.2 (7.2, 7.5)	1.000
Morphologically normal sperm, %	7.47 ± 2.87	6.01 ± 1.78	0.132

(Figure 2A) and C9orf72 protein expression ($p<0.001$) (Figure 2B and C). Furthermore, cell viability significantly decreased ($p<0.001$) (Figure 2D), while apoptosis rate and ROS levels were significantly increased ($p<0.001$) (Figure 2E and F). Importantly, no significant differences were observed between the CON and NC groups across all measured parameters ($p>0.05$), indicating that lentiviral infection at an MOI of 20 and empty vector expression did not affect GC-1 spg cell viability, apoptosis, or ROS levels, thereby excluding potential cytotoxic effects of the viral delivery itself. Thus, the observed reduction in cell viability, together with increased apoptosis and elevated ROS levels, was specifically associated with C9orf72 overexpression rather than nonspecific viral toxicity.

C9orf72 overexpression is associated with impaired energy metabolism in GC-1 spg cells

The levels of fructose, GAPDH enzymatic activity, and the intracellular concentrations of NADH and NAD^+ in GC-1 spg cells were quantified using ELISA. Glycolysis-associated

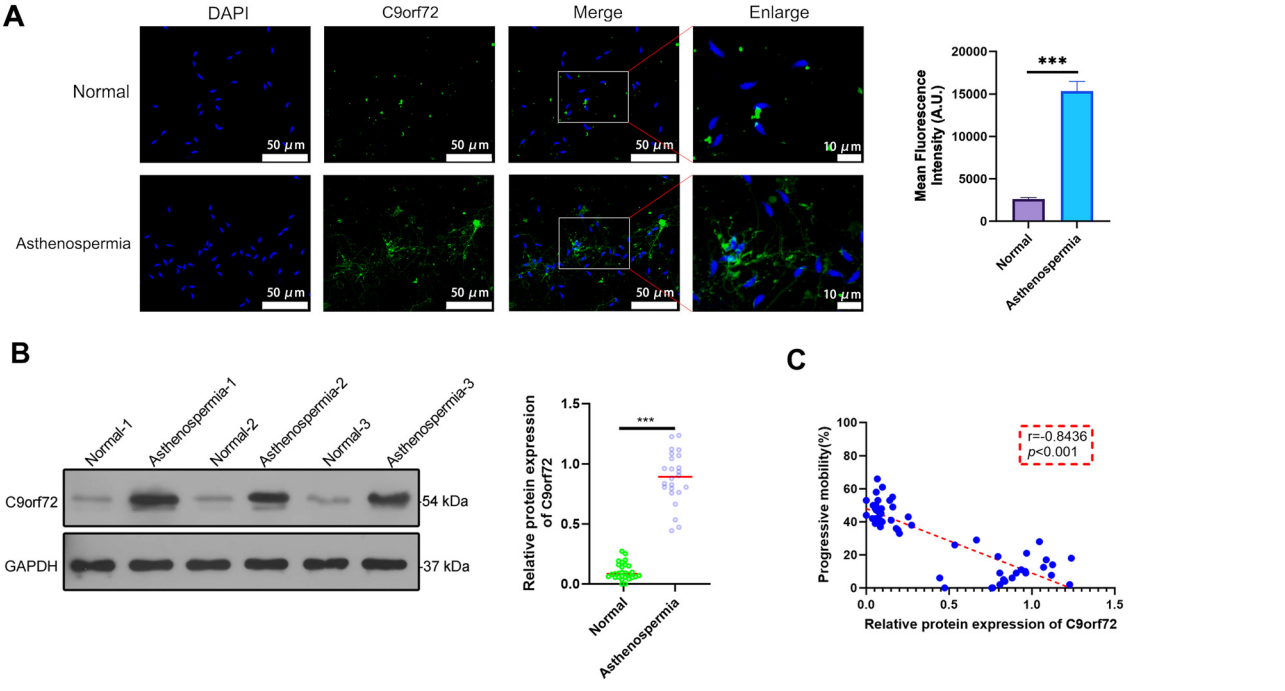

Figure 1: Elevated C9orf72 expression in asthenozoospermia semen and its inverse correlation with sperm progressive motility. A: Immunofluorescence showing the expression of C9orf72 protein (magnification 1,500×) and was quantified using mean fluorescence intensity from three regions. B: C9orf72 expression levels detection via Western blot. C: Pearson correlation analysis. Data are presented as mean±SD. Statistical analysis was performed using Student's t-test and Pearson correlation. Compared with the normal group, *** $p<0.001$. Normal group: semen samples from healthy controls (n=28). Asthenozoospermia group: semen samples from asthenozoospermia patients (n=24).

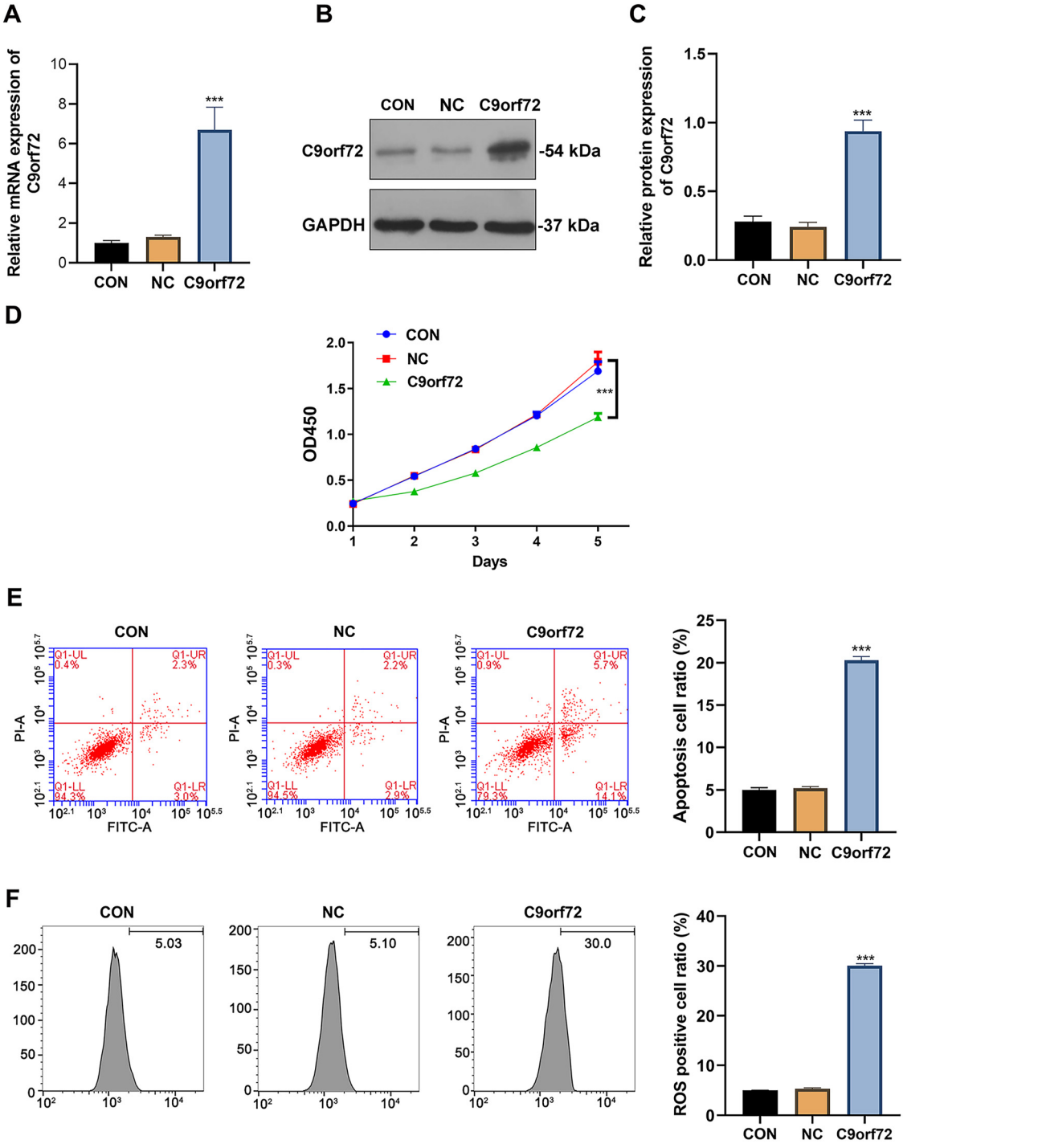

Figure 2: C9orf72 overexpression inhibits proliferation of GC-1 spg cells. A: RT-PCR showing relative mRNA expression of C9orf72; B: Western blot showing C9orf72 protein expression; C: Grayscale analysis and statistical evaluation; D: CCK-8 assay to assess cell viability; E: Flow cytometry analysis of cell apoptosis; F: Flow cytometry analysis of ROS levels. Data are presented as mean±SD. All experiments were repeated three times (n=3). Statistical analysis was performed using one-way ANOVA. *** $p<0.001$ compared to NC group. CON: Control group. NC: Negative control vector transfection group. C9orf72: C9orf72 overexpression group.

protein expression was examined via Western blot, while the OCR was evaluated using the Seahorse XF extracellular flux analyzer. At 24 h post-transduction with the C9orf72-overexpressing lentivirus, cells exhibited a significant elevation in fructose concentration compared to the NC group ($p<0.001$; Figure 3A). In contrast, GAPDH activity was

markedly reduced in the overexpression group ($p<0.001$; Figure 3B). Furthermore, C9orf72 overexpression led to a substantial downregulation of key glycolytic proteins, including GLUT1, GLUT3, HK2, and LDHA ($p<0.001$; Figure 3C). NADH/NAD$^+$ ratio was significantly increased in the C9orf72 group ($p<0.001$; Figure 3D), implying disruption of redox homeostasis and energy metabolism. Analysis of OCR revealed a notable decline in mitochondrial respiratory function in the overexpression group. After oligomycin injection, ATP-linked respiration was significantly reduced, while FCCP stimulation failed to induce maximal respiration as in the controls, indicating impaired OXPHOS capacity ($p<0.001$; Figure 3E). Quantification of maximal respiration confirmed this effect, as C9orf72-overexpressing cells exhibited a significant reduction compared with CON and NC groups ($p<0.001$; Figure 3F). Final injection of rotenone/antimycin A confirmed that the residual OCR was non-mitochondrial. In contrast, no significant differences were found between the CON and NC groups in any of these metabolic indices ($p>0.05$). These results suggest that C9orf72 overexpression is associated with impaired energy metabolism in GC-1 spg cells, particularly by disrupting fructose metabolism and mitochondrial respiration.

C9orf72 overexpression is associated with reduced mitophagy in GC-1 spg cells

GC-1 spg cells were transduced with C9orf72 overexpression lentivirus or NC. LC3-labeled autophagosomes and TOM20-labeled mitochondria were observed to assess changes in autophagosome and mitochondria co-localization and quantity. Compared to the CON and NC groups, C9orf72 overexpression resulted in decreased LC3 green fluorescence, reducing autophagosome formation, and decreased co-localization of autophagosomes with mitochondria (yellow) (Figure 4), suggesting that C9orf72 overexpression is associated with reduced mitophagy in GC-1 spg cells. This observation was further supported by quantitative colocalization analysis using Pearson's correlation

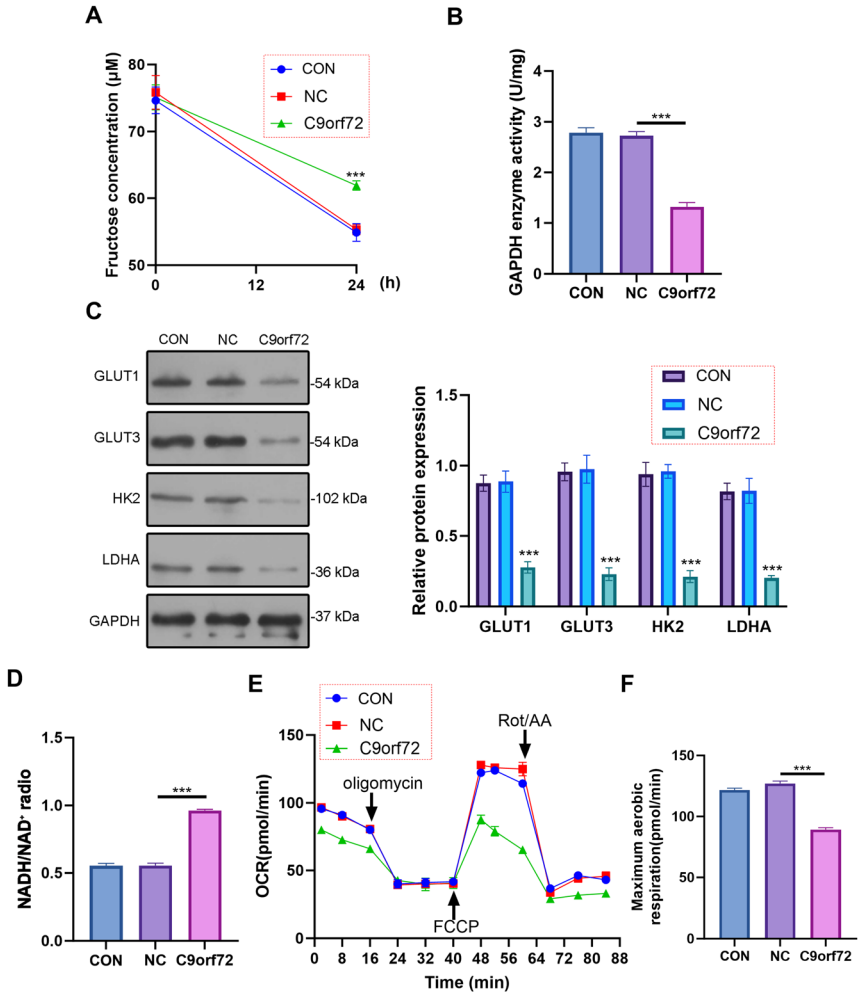

Figure 3: C9orf72 overexpression inhibits energy metabolism and expression of glycolysis-related proteins in GC-1 spg cells. A: Fructose concentration measurements at 0 and 24 h; B: ELISA analysis of GAPDH enzyme activity; C: Western blot of glycolysis-related proteins; D: ELISA analysis of NADH/NAD$^+$ ratio; E: Seahorse XF analysis of oxygen consumption rate (OCR); sequential injections were performed with oligomycin (1 μM, ~16 min; ATP synthase inhibitor to measure ATP-linked respiration), FCCP (1.5 μM, ~40 min; uncoupler to reveal maximal respiration capacity), and rotenone/antimycin A (1 μM each, ~60 min; complex I/III inhibitors to define non-mitochondrial respiration). OCR values were normalized to total protein content. F: Bar graphs summarizing basal respiration and maximal respiration derived from OCR curves. Data are presented as mean±SD. All experiments were repeated three times (n=3). Statistical analysis was performed using one-way ANOVA or two-way ANOVA. ***$p<0.001$ compared to NC group. CON: Control group. NC: Negative control vector transfection group. C9orf72: C9orf72 overexpression group.

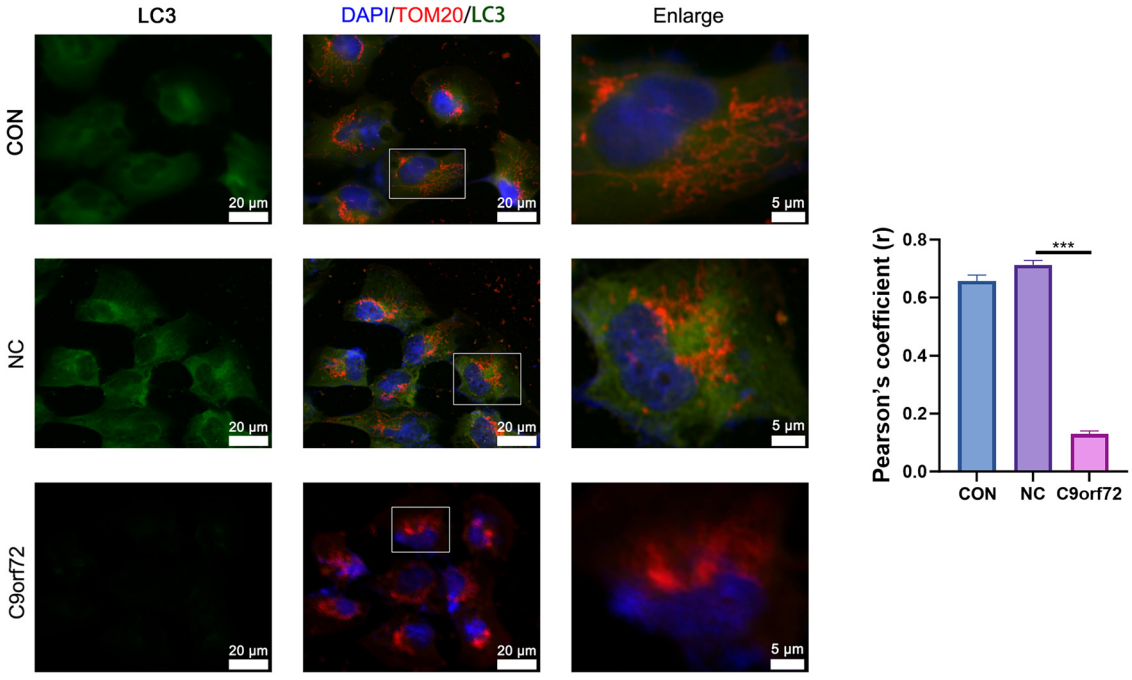

Figure 4: C9orf72 overexpression inhibits mitophagy in GC-1 spg cells LC3 (green)–labeled autophagosomes and TOM20 (red)–labeled mitochondria were visualized, and colocalization was quantified using Pearson's coefficient from three regions. Magnification: 1,500 and 5,000×. All experiments were repeated three times (n=3). Data are presented as mean±SD. Statistical analysis was performed using one-way ANOVA. ***p<0.001 compared to NC group. CON: Control group. NC: Negative control vector transfection group. C9orf72: C9orf72 overexpression group.

coefficient, which showed a significant reduction in LC3/TOM20 overlap in the C9orf72 group compared with Control ($p<0.001$), consistent with impaired mitophagy (Figure 4, right panel).

C9orf72–LC3 interaction and its association with impaired mitophagy in GC-1 spg cells

The interaction between C9orf72 and LC3 was analyzed by molecular docking and co-immunoprecipitation experiments. The direct interaction between C9orf72 and LC3 was further validated by co-immunoprecipitation. Molecular docking analysis revealed that the binding sites between C9orf72 and LC3 include multiple amino acid residues (e.g., His-128, Asp-48), with several residues forming hydrogen bonds, such as the hydrogen bond between HIS65 of C9orf72 and GLN22 of LC3. These amino acid sites may play a key role in their interaction (Figure 5A). Co-immunoprecipitation experiments showed that C9orf72 was successfully detected in the LC3 immunoprecipitate, while no C9orf72 precipitation was observed in the IgG control group, indicating a specific interaction between the two proteins (Figure 5B). Furthermore, site-directed mutagenesis combined with co-immunoprecipitation demonstrated that the LC3 protein signal bound to all four mutants (H65A, H128A, K83A, and K422A) was significantly reduced compared with wild-type C9orf72 ($p<0.001$). Notably, the reduction was most pronounced in the H128A mutants, indicating that His-128 is critical residues for maintaining the C9orf72–LC3 interaction, while His-65, Lys83 and Lys-422 also contribute to the binding (Figure 5C).

To further validate the functional relevance of this interaction, rescue experiments were performed by co-expressing LC3 in C9orf72-overexpressing GC-1 cells. Compared with the NC group, C9orf72 overexpression markedly reduced LC3/TOM20 co-localization and impaired mitophagy ($p<0.001$) (Figure 6A), significantly suppressed cell proliferation ($p<0.001$) (Figure 6B), increased extracellular fructose accumulation ($p<0.001$) (Figure 6C), and decreased GAPDH enzymatic activity ($p<0.001$) (Figure 6D). Importantly, LC3 overexpression partially rescued these phenotypes, restoring LC3/TOM20 colocalization and improving metabolic parameters. These findings support that C9orf72 overexpression correlates with impaired mitophagy and fructose metabolism, potentially through suppression of LC3, and that enhancing LC3 expression can counteract these effects.

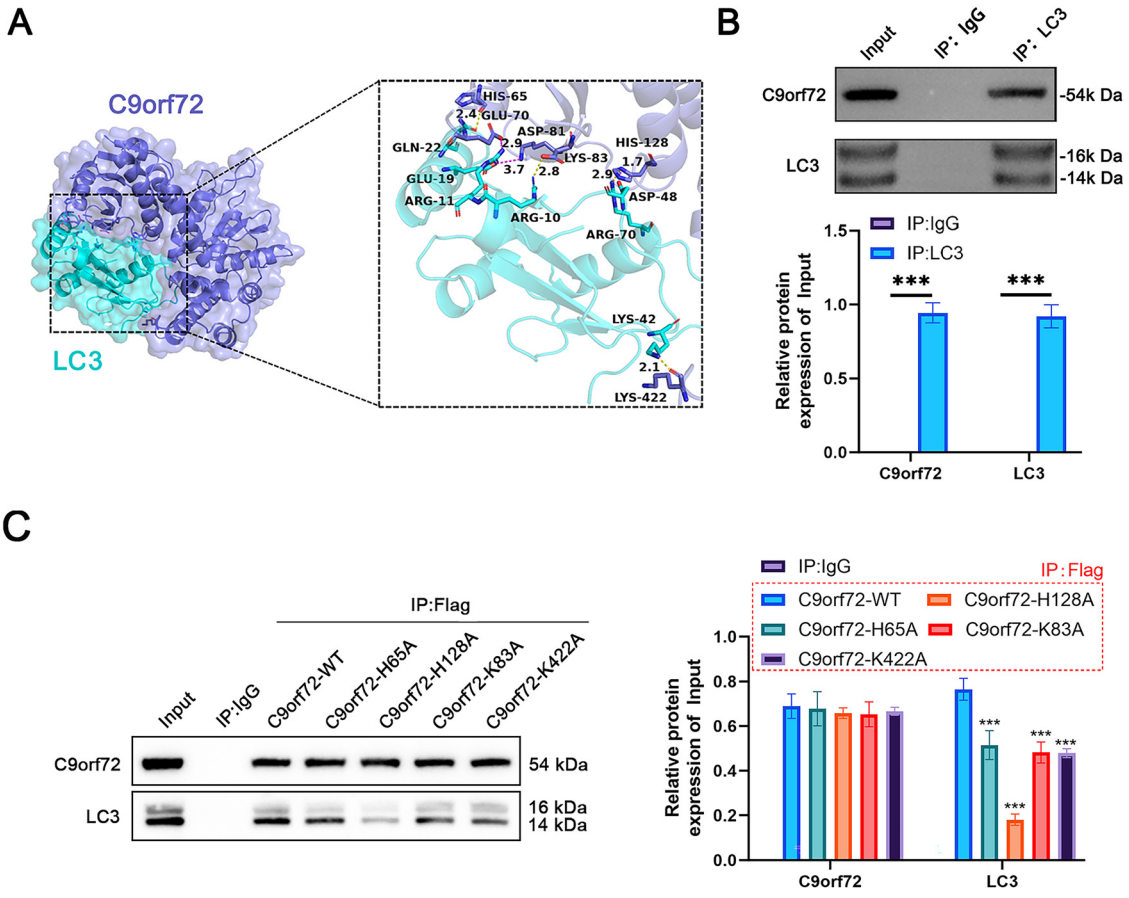

Figure 5: C9orf72 interacts with LC3 in GC-1 spg cells A: molecular docking analysis of the interaction sites between C9orf72 and LC3; B: Co-immunoprecipitation of C9orf72 and LC3; C: site-directed mutagenesis and co-immunoprecipitation analysis of C9orf72 wild-type (WT) and mutants (H65A, H128A, K83A, and K422A) with LC3. All experiments were repeated three times (n=3). Data are presented as mean±SD. Statistical analysis was performed using one-way ANOVA. ***p<0.001 compared to C9orf72-WT group.

Discussion

Previous studies reported that C9orf72 mRNA expression is elevated in asthenozoospermia [16], and our results confirm that C9orf72 is markedly upregulated in semen and inversely correlated with progressive motility. Elevated C9orf72 expression has also been linked to non-obstructive azoospermia [35]. Our findings suggest a potential role of C9orf72 in asthenozoospermia, although mechanistic validation is still lacking. C9orf72 was detected in both the sperm head and tail, implying involvement in motility- and head-related functions. Its localization may influence key processes such as the acrosome reaction, which is essential for fertilization [36]. Thus, C9orf72 overexpression may be associated with alterations in motility-related pathways, but further studies are required. Using GC-1 spg cells, we also examined how C9orf72 affects cell proliferation and metabolism, providing insight into its potential role in the pathogenesis of asthenozoospermia.

Spermatogonia are the foundational germ cell population of the seminiferous epithelium, responsible for maintaining the stem cell pool, balancing self-renewal and differentiation, and initiating meiosis to ensure continuous sperm production [37, 38]. Transcriptomic analyses show that GC-1 spermatogonia retain key features of type B spermatogonia and share overlap with spermatocyte gene expression, making them a relevant model for early spermatogenic events [39]. Cross-species studies further reveal that spermatogonia are enriched in conserved gene networks regulating RNA, metabolism, and meiosis, highlighting their central role in spermatogenesis and male infertility [37]. The use of GC-1 spg cells as an *in vitro* model is well established. Prior studies have shown their applicability in spermatogenesis and energy metabolism research, including levocarnitine improving spermatogenic dysfunction via PI3K/AKT signaling [40], substance P stimulating their proliferation through Erk1/2 signaling

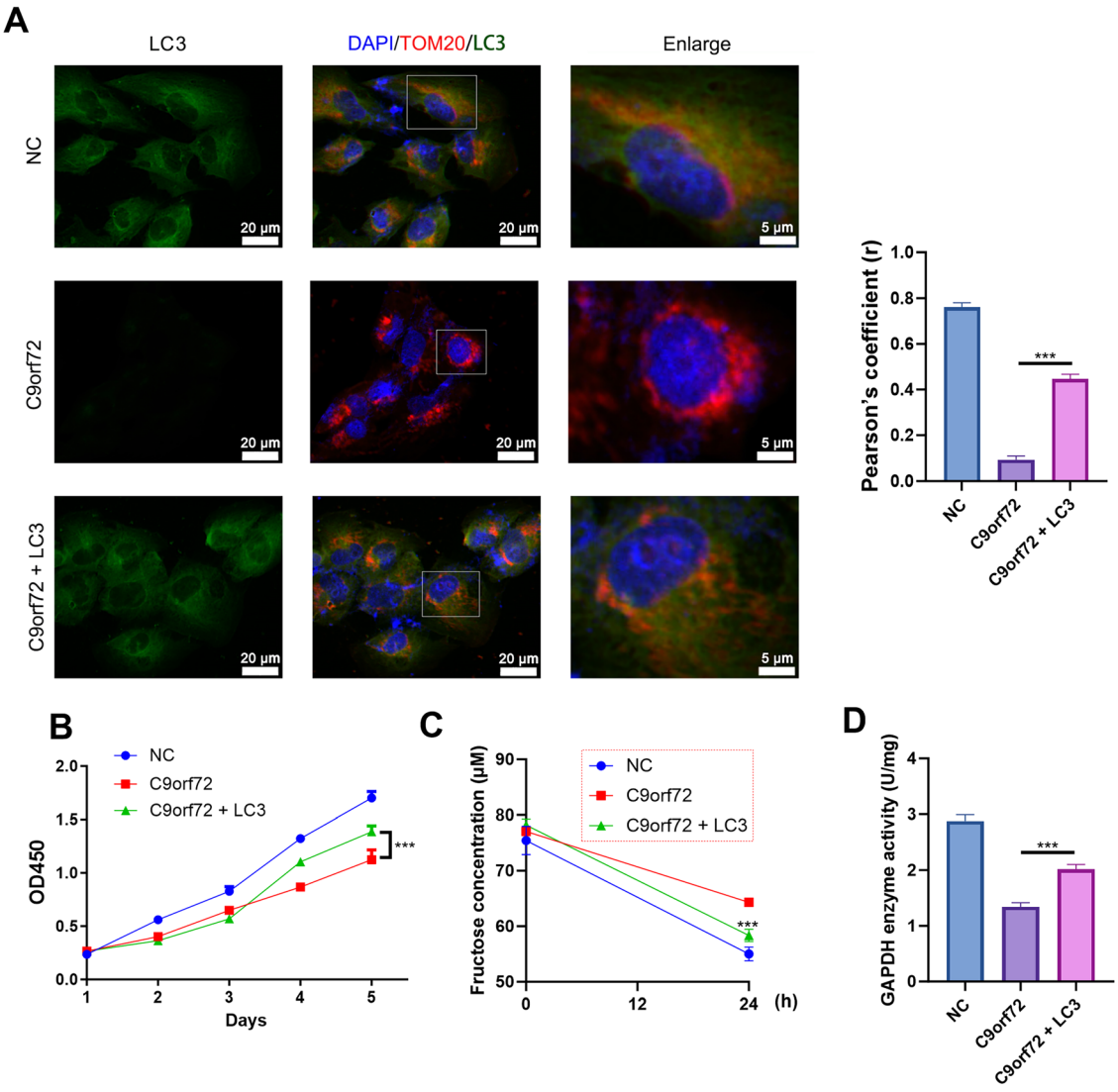

Figure 6: LC3 overexpression rescues C9orf72-induced defects in mitophagy and fructose metabolism A: Representative immunofluorescence images showing LC3 (green), TOM20 (red), and nuclei (blue, DAPI) in GC-1 spg cells, Scale bar=20 μm. Quantification of colocalization was assessed using Pearson's coefficient (right panel). B: Cell proliferation was assessed by CCK-8 assay over 5 days. C: Fructose concentrations in the culture medium measured at 0, and 24 h. D: GAPDH enzymatic activity assay. Data are presented as mean±SD. All experiments were repeated three times (n=3). Statistical analysis was performed using one-way ANOVA. $^{***}p<0.001$ compared to C9orf72 group. NC: Negative control vector transfection group. C9orf72: C9orf72 overexpression group. C9orf72 + LC3: C9orf72 and LC3 overexpression group.

[32], and miR-27b-3p protecting against high glucose–induced damage by regulating Gfpt1/HBP signaling [25]. Moreover, Sertoli cell–secreted FGF-2 has been reported to regulate glycolysis in GC-1 spg cells through the MEK/ERK/CREB pathway [41], supporting their rational use in studies of spermatogenesis and metabolism. Spermatogonia display unique responses to stress, including oxidative injury and ferroptosis. Mitochondrial dysfunction, elevated ROS, and altered autophagy are hallmarks of spermatogonial damage under toxic or metabolic stress [42, 43]. Metabolically, they shift from OXPHOS-dominated energy production in gonocytes to a more glycolytic phenotype during maturation, accompanied by mitochondrial remodeling and regulators such as UCP2 and PLZF [44]. In our study, C9orf72 overexpression in GC-1 cells suppressed proliferation, increased apoptosis, and elevated ROS. Excessive ROS, often arising from mitochondrial dysfunction, compromises ATP production and triggers cell death [45–47]. Consistent with this, C9orf72 overexpression was associated with increased ROS, enhanced apoptosis, and reduced proliferation. ROS accumulation is a well-known contributor to male

infertility, as it promotes lipid peroxidation, protein oxidation, and DNA fragmentation, ultimately impairing sperm integrity and motility [48, 49]. Our findings suggest that C9orf72 may contribute to impaired spermatogonial proliferation through effects on fructose metabolism and mitochondrial function. Given the established role of oxidative stress in asthenozoospermia, potential therapeutic strategies include antioxidants, metabolic modulators, and mitophagy-targeted interventions to restore mitochondrial quality and sperm function [50–52].

Mitochondrial homeostasis, especially the maintenance of membrane potential (ΔΨm), is essential for sperm motility, hyperactivation, energy metabolism, acrosomal exocytosis, and genomic stability [53, 54]. Disruption of mitochondrial bioenergetics reduces ATP production for flagellar movement and may contribute to asthenozoospermia [4]. C9orf72 has been reported to regulate autophagosome formation through coordination with the Rab1a–ULK1 complex [19]. In animal studies, Shengjing Tablets improved asthenozoospermia by enhancing mitochondrial ubiquitination and mitophagy via the LKB1/AMPK/ULK1 pathway [55]. In our study, C9orf72 overexpression inhibited mitophagy in GC-1 spg cells and directly interacted with LC3. LC3 facilitates the recruitment of mitochondria into autophagosomes for degradation, thereby preserving mitochondrial quality and energy metabolism [56]. In aging mouse epididymis, reduced LC3–LAMP2 colocalization indicated impaired mitophagy, which may compromise sperm quality [57]. C9orf72 overexpression decreased LC3 fluorescence and autophagosome formation, while co-immunoprecipitation confirmed its direct interaction with LC3 and identified key binding residues. These assays do not prove that C9orf72 induces LC3 degradation but suggest that C9orf72 may influence LC3 function through both reduced LC3 levels and direct protein interaction. Taken together, our findings indicate that impaired mitophagy may underlie the inhibitory effects of C9orf72 on GC-1 spg cell proliferation, though further mechanistic studies are needed.

Mitochondria are the main sites of fructose metabolism and ATP production, while mitophagy regulates intracellular fructose utilization [58]. Fructose-derived ATP supports sperm functions such as motility, hyperactivation, acrosomal exocytosis, and homeostasis [59]. Fructose enters glycolysis through hexokinase-mediated phosphorylation [60, 61]. In our study, C9orf72 overexpression caused fructose accumulation in the medium, reduced GAPDH activity, and elevated the $NADH/NAD^+$ ratio. It also downregulated glucose transporters (GLUT1, GLUT3) and glycolytic enzymes (HK2, LDHA), indicating disruption of energy balance. The reduction in GAPDH activity despite unchanged protein levels may reflect oxidative stress–induced modifications, such as S-nitrosylation or carbonylation, that impair enzyme function [62, 63]. These findings suggest that C9orf72 modulates fructose metabolism and may contribute to energy insufficiency in asthenozoospermia.

Supporting evidence comes from Drosophila studies, where a high-sugar diet reduced GAPDH activity, increased the $NADH/NAD^+$ ratio, and disrupted fructose metabolism [64]. Similarly, an elevated $NADH/NAD^+$ ratio has been linked to oxidative stress, mitochondrial dysfunction, and impaired homeostasis [65]. Although we observed increased ROS levels, it remains unclear whether this reflects a direct effect of C9orf72 or a secondary consequence of metabolic impairment. In this study, C9orf72 overexpression was associated with elevated ROS levels. However, it remains unclear whether this increase reflects a direct effect of C9orf72 or a secondary consequence of impaired glycolysis and mitochondrial dysfunction. The absence of rescue experiments using ROS scavengers such as N-acetylcysteine (NAC) represents a limitation of our study, and future work will be required to delineate the causal relationship.

Although semen washing removes seminal plasma, non-sperm cells such as leukocytes may remain, and C9orf72 is also expressed in leukocytes [66]. Thus, the observed overexpression in asthenozoospermia samples may partly originate from leukocytes, and future studies should include leukocyte-specific markers (e.g., CD45) to confirm the cellular source. Another limitation is the use of GC-1 spg cells, which differ from mature human sperm in physiology, metabolism, and developmental context [67]. Validation in human-derived samples is therefore required. The sample size was smaller than recommended by clinical research guidelines (24 patients vs. 63 per group), which may have reduced statistical power; thus, the results should be considered exploratory and confirmed in larger cohorts. The evidence for C9orf72–LC3 interaction is preliminary, as docking and co-immunoprecipitation cannot rule out indirect binding. Further mutational and *in situ* validation studies are needed. In addition, clinical data on lifestyle factors and comorbidities were not systematically collected, which may confound the findings. Finally, the absence of *in vivo* validation represents another limitation. Mouse models with C9orf72 overexpression or knockout will be important to confirm its role in mitophagy and sperm function. Moreover, downstream signaling pathways, such as the PINK1/Parkin axis, should be investigated to clarify the mechanisms and strengthen translational relevance.

In conclusion, this study demonstrates that C9orf72 expression is elevated in asthenozoospermic semen and

shows a negative association with sperm progressive motility. Functional analyses in GC-1 spg cells revealed that C9orf72 overexpression is linked to suppressed cell proliferation, disrupted fructose metabolism, oxidative stress, and reduced mitophagy, partly through its interaction with LC3. These findings highlight a potential role of C9orf72 as a regulator of sperm energy metabolism and mitochondrial quality control, providing new mechanistic insight into the pathogenesis of asthenozoospermia.

Funding information: This work was supported by the Hainan Provincial Natural Science Foundation (822RC857), the Key Research and Development Program of Hainan Province (ZDYF2023SHFZ093), the Hainan Province Clinical Medical Center (QWYH202175), the Excellent Talent Team Program of Hainan Province (QRCBT202121), Hainan Women and Children's Medical Center "1126 Plan"(QFY202416-1126-BJ-02) and the Wu Jieping Medical Foundation (320.6750.2024-06-17).

Authors contributions: Hui Lu designed and performed most experiments, analyzed data, and drafted the manuscript. Dongchuan Xu assisted in cell experiments, lentiviral construction, and RT-PCR. Liqiang Zhao collected semen samples, performed semen analysis, and assisted in data interpretation. Hailing Ruan contributed to Western blot, RT-PCR, and ELISA. Anguo Wang assisted in ROS detection and Seahorse analysis. Yejuan Li supported co-immunoprecipitation and sample processing. Weiying Lu conceptualized and supervised the study and revised the manuscript as corresponding author. All authors approved the final manuscript.

Conflict of interest: The authors declare that they have no conflicts of interest.

Data availability statement: The datasets used and/or analyzed during the present study are available from the corresponding author on reasonable request.

References

1. Pereira R, Sousa M. Morphological and molecular bases of male infertility: a closer look at sperm flagellum. Genes 2023;14:383.
2. Cooper TG, Noonan E, Von Eckardstein S, Auger J, Baker HW, Behre HM, et al. World health organization reference values for human semen characteristics. Hum Reprod Update 2010;16:231–45.
3. Zhou Y, Yao W, Zhang D, Yu Y, Chen S, Lu H, et al. Effectiveness of acupuncture for asthenozoospermia: a protocol for systematic review and meta-analysis. Medicine (Baltim) 2021;100:e25711.
4. Durairajanayagam D, Singh D, Agarwal A, Henkel R. Causes and consequences of sperm mitochondrial dysfunction. Andrologia 2021; 53:e13666.
5. Minhas S, Bettocchi C, Boeri L, Capogrosso P, Carvalho J, Cilesiz NC, et al. European association of urology guidelines on Male sexual and reproductive health: 2021 update on male infertility. Eur Urol 2021;80: 603–20.
6. Yang YT, Yan B, Guo LN, Liu M, Li YH, Shao ZY, et al. Scriptaid is a prospective agent for improving human asthenozoospermic sample quality and fertilization rate in vitro. Asian J Androl 2024;26:490–9.
7. Yang YT, Yan B, Li YH, Guo LN, Wang WW, Liu LJ, et al. Phosphodiesterase 10A inhibitor PF-2545920 as a prospective agent for the clinical promotion of sperm motility. Asian J Androl 2023;25: 608–15.
8. Kiani AK, Paolacci S, Scanzano P, Michelini S, Capodicasa N, D'agruma L, et al. Complications related to in vitro reproductive techniques support the implementation of natural procreative technologies. Acta Biomed 2020;91:e2020018.
9. Vertika S, Singh KK, Rajender S. Mitochondria, spermatogenesis, and Male infertility – an update. Mitochondrion 2020;54:26–40.
10. Barbagallo F, La Vignera S, Cannarella R, Aversa A, Calogero AE, Condorelli RA. Evaluation of sperm mitochondrial function: a key organelle for sperm motility. J Clin Med 2020;9:363.
11. Costa J, Braga PC, Rebelo I, Oliveira PF, Alves MG. Mitochondria quality control and Male fertility. Biology 2023;12:827.
12. Rotimi DE, Iyobhebhe M, Oluwayemi ET, Evbuomwan IO, Asaleye RM, Ojo OA, et al. Mitophagy and spermatogenesis: role and mechanisms. Biochem Biophys Rep 2024;38:101698.
13. Escada-Rebelo S, Cristo MI, Ramalho-Santos J, Amaral S. Mitochondria-targeted compounds to assess and improve human sperm function. Antioxidants Redox Signal 2022;37:451–80.
14. Luo ZY, Jiang TX, Zhang T, Xu P, Qiu XB. Ubiquitin ligase Nrdp1 controls autophagy-associated acrosome biogenesis and mitochondrial arrangement during spermiogenesis. Cells 2023;12:2211.
15. Choong CJ, Okuno T, Ikenaka K, Baba K, Hayakawa H, Koike M, et al. Alternative mitochondrial quality control mediated by extracellular release. Autophagy 2021;17:2962–74.
16. Lu H, Xu D, Wang P, Sun W, Xue X, Hu Y, et al. RNA-sequencing and bioinformatics analysis of long noncoding RNAs and mRNAs in the asthenozoospermia. Biosci Rep 2020;40:BSR20194041.
17. Smeyers J, Banchi EG, Latouche M. C9ORF72: what it is, what it does, and why it matters. Front Cell Neurosci 2021;15:661447.
18. Pang W, Hu F. Cellular and physiological functions of C9ORF72 and implications for ALS/FTD. J Neurochem 2021;157:334–50.
19. Webster CP, Smith EF, Bauer CS, Moller A, Hautbergue GM, Ferraiuolo L, et al. The C9orf72 protein interacts with Rab1a and the ULK1 complex to regulate initiation of autophagy. EMBO J 2016;35:1656–76.
20. Yang M, Liang C, Swaminathan K, Herrlinger S, Lai F, Shiekhattar R, et al. A C9ORF72/SMCR8-containing complex regulates ULK1 and plays a dual role in autophagy. Sci Adv 2016;2:e1601167.
21. Wang T, Liu H, Itoh K, Oh S, Zhao L, Murata D, et al. C9orf72 regulates energy homeostasis by stabilizing mitochondrial complex I assembly. Cell Metab 2021;33:531–46.e9.
22. Oakes JA, Davies MC, Collins MO. TBK1: a new player in ALS linking autophagy and neuroinflammation. Mol Brain 2017;10:5.
23. Gruhl SL, Ho LM, Sim MYX, Lee SN, Yu SL, Yong TT, et al. Seminal biomarkers and their correlations to semen parameters in subfertile men. Eur J Obstet Gynecol Reprod Biol X 2023;19:100229.
24. Yuan Q, Hong R, Ni Y, Jiang M, Liu J, Chen Z, et al. Correlation between seminal plasma biochemical markers and semen parameters in idiopathic oligoasthenoteratospermia: identification of biomarkers for L-carnitine therapy. Front Endocrinol 2024;15:1330629.
25. Zheng H, Huang J, Zhang M, Zhao HJ, Chen P, Zeng ZH. miR-27b-3p improved high glucose-induced spermatogenic cell damage via regulating Gfpt1/HBP signaling. Eur Surg Res 2022;63:64–76.

26. Tian Y, Xiao YH, Geng T, Sun C, Gu J, Tang KF, et al. Clusterin suppresses spermatogenic cell apoptosis to alleviate diabetes-induced testicular damage by inhibiting autophagy via the PI3K/AKT/mTOR axis. Biol Cell 2021;113:14–27.
27. Serdar CC, Cihan M, Yücel D, Serdar MA. Sample size, power and effect size revisited: simplified and practical approaches in pre-clinical, clinical and laboratory studies. Biochem Med 2021;31:010502.
28. Ranganathan P, Deo V, Pramesh CS. Sample size calculation in clinical research. Perspect Clin Res 2024;15:155–9.
29. Lu JC, Huang YF, Lü NQ. WHO laboratory manual for the examination and processing of human semen: its applicability to andrology laboratories in China. Zhonghua Nan Ke Xue 2010;16:867–71.
30. Wu W, Guo X, Li J, Yang M, Xiong Y. Comparison of different processed products of Allium tuberosum rottler for the treatment of mice asthenozoospermia. Transl Androl Urol 2024;13: 2209–28.
31. Adler J, Parmryd I. Quantifying colocalization by correlation: the pearson correlation coefficient is superior to the Mander's overlap coefficient. Cytometry A 2010;77:733–42.
32. Chen Z, Liu M, Hu JH, Gao Y, Deng C, Jiang MH. Substance P restores spermatogenesis in busulfan-treated mice: a new strategy for Male infertility therapy. Biomed Pharmacother 2021;133:110868.
33. Li C, Cheng D, Xu P, Nie H, Zhang T, Pang X. POSTN promotes the proliferation of spermatogonial cells by activating the Wnt/β-Catenin signaling pathway. Reprod Sci 2021;28:2906–15.
34. Plitzko B, Loesgen S. Measurement of oxygen consumption rate (OCR) and extracellular acidification rate (ECAR) in culture cells for assessment of the energy metabolism. Bio Protoc 2018;8:e2850.
35. Luo X, Zheng H, Nai Z, Li M, Li Y, Lin N, et al. Identification of biomarkers associated with macrophage infiltration in non-obstructive azoospermia using single-cell transcriptomic and microarray data. Ann Transl Med 2023;11:55.
36. Breitbart H, Grinshtein E. Mechanisms that protect mammalian sperm from the spontaneous acrosome reaction. Int J Mol Sci 2023; 24:17005.
37. Wang X, Cheng L, Lu X, Jin H, Cui L, Guo Y, et al. Cross-species comparative single-cell transcriptomics highlights the molecular evolution and genetic basis of male infertility. Cell Rep 2025;44: 115118.
38. Li X, Long XY, Xie YJ, Zeng X, Chen X, Mo ZC. The roles of retinoic acid in the differentiation of spermatogonia and spermatogenic disorders. Clin Chim Acta 2019;497:54–60.
39. Verma P, Parte P. Revisiting the characteristics of testicular germ cell lines GC-1(spg) and GC-2(spd)ts. Mol Biotechnol 2021;63:941–52.
40. Wang J, Bao B, Meng F, Deng S, Dai H, Feng J, et al. The mechanism analysis using PI3K/AKT pathway for the effects of levocarnitine in the treatment of spermatogenic dysfunction. Andrologia 2022;54: e14290.
41. Gómez M, Manzano A, Figueras A, Viñals F, Ventura F, Rosa JL, et al. Sertoli-secreted FGF-2 induces PFKFB4 isozyme expression in mouse spermatogenic cells by activation of the MEK/ERK/CREB pathway. Am J Physiol Endocrinol Metab 2012;303:E695–707.
42. Jia D, Huang W, Yin Q, Wang H, Wang Z, Zhang M, et al. Melatonin alleviates ferroptosis triggered by cadmium via regulating ferritinophagy and iron metabolism in spermatogonia. Sci Rep 2025;15: 8910.
43. Wang X, Huang S, Zhao Y, Chen H, Yan L, Ge H, et al. Activation of autophagy is required for clearance of mitochondrial ROS in patients with asthenozoospermia. PeerJ 2025;13:e18827.
44. Voigt AL, Kondro DA, Powell D, Valli-Pulaski H, Ungrin M, Stukenborg JB, et al. Unique metabolic phenotype and its transition during maturation of juvenile male germ cells. FASEB J 2021;35:e21513.
45. Schieber M, Chandel NS. ROS function in redox signaling and oxidative stress. Curr Biol 2014;24:R453–62.
46. Rani V, Deep G, Singh RK, Palle K, Yadav UC. Oxidative stress and metabolic disorders: pathogenesis and therapeutic strategies. Life Sci 2016;148:183–93.
47. Belousov DM, Mikhaylenko EV, Somasundaram SG, Kirkland CE, Aliev G. The dawn of mitophagy: what do we know by now? Curr Neuropharmacol 2021;19:170–92.
48. Wang Y, Fu X, Li H. Mechanisms of oxidative stress-induced sperm dysfunction. Front Endocrinol 2025;16:1520835.
49. Gill K, Machałowski T, Harasny P, Grabowska M, Duchnik E, Piasecka M. Low human sperm motility coexists with sperm nuclear DNA damage and oxidative stress in semen. Andrology 2024;12:1154–69.
50. Tiwari S, Dewry RK, Srivastava R, Nath S, Mohanty TK. Targeted antioxidant delivery modulates mitochondrial functions, ameliorates oxidative stress and preserve sperm quality during cryopreservation. Theriogenology 2022;179:22–31.
51. O'flaherty C, Scarlata E. Oxidative stress and reproductive function: the protection of mammalian spermatozoa against oxidative stress. Reproduction 2022;164:F67–78.
52. Boonsimma K, Ngeamvijawat J, Sukcharoen N, Boonla C. Supplementing post-wash asthenozoospermic human spermatozoa with coenzyme Q10 for 1 hr in vitro improves sperm motility, but not oxidative stress. Andrologia 2020;52:e13818.
53. Meyers S, Bulkeley E, Foutouhi A. Sperm mitochondrial regulation in motility and fertility in horses. Reprod Domest Anim 2019;54:22–8.
54. Bulkeley EA, Foutouhi A, Wigney K, Santistevan AC, Collins C, Mcnabb B, et al. Effects from disruption of mitochondrial electron transport chain function on bull sperm motility. Theriogenology 2021;176:63–72.
55. Li G, Xu Y, Li Y, Chang D, Zhang P, Ma Z, et al. Qiangjing tablets ameliorate asthenozoospermia via mitochondrial ubiquitination and mitophagy mediated by LKB1/AMPK/ULK1 signaling. Pharm Biol 2023; 61:271–80.
56. Towers CG, Wodetzki DK, Thorburn J, Smith KR, Caino MC, Thorburn A. Mitochondrial-derived vesicles compensate for loss of LC3-mediated mitophagy. Dev Cell 2021;56:2029–42. e5.
57. Liu C, Wu C, Zhang S, Lv Z. Contribution of impaired autophagy, mitochondrial dysfunction and abnormal lipolysis to epididymal aging in mice. Exp Gerontol 2024;195:112528.
58. Miyazaki N, Shiratori R, Oshima T, Zhang Z, Valencia R, Kranrod J, et al. PINK1-dependent and Parkin-independent mitophagy is involved in reprogramming of glycometabolism in pancreatic cancer cells. Biochem Biophys Res Commun 2022;625:167–73.
59. Mukai C, Travis AJ. What sperm can teach us about energy production. Reprod Domest Anim 2012;47:164–9.
60. Davis ME, Mc CW. Fructolysis of human spermatozoa. Fertil Steril 1950; 1:362–72.
61. Jones AR, Connor DE. Fructose metabolism by mature boar spermatozoa. Reprod Fertil Dev 2000;12:355–9.
62. Tristan C, Shahani N, Sedlak TW, Sawa A. The diverse functions of GAPDH: views from different subcellular compartments. Cell Signal 2011;23:317–23.
63. Tossounian MA, Zhang B, Gout I. The writers, readers, and erasers in redox regulation of GAPDH. Antioxidants 2020;9:1288.
64. Moon SJ, Hu Y, Dzieciatkowska M, Kim AR, Chen PL, Asara JM, et al. Identification of high sugar diet-induced dysregulated metabolic pathways in muscle using tissue-specific metabolic models in

Drosophila. bioRxiv 2024:591006. https://doi.org/10.1101/2024.04.24.591006.
65. Yan LJ. NADH/NAD(+) redox imbalance and diabetic kidney disease. Biomolecules 2021;11:730.
66. Shpilyukova YA, Fedotova EY, Abramycheva NY, Kochergin IA, Zakroyshchikova IV, Zakharova MN, et al. C9orf72 gene expression in frontotemporal dementia and amyotrophic lateral sclerosis. Bull Exp Biol Med 2020;169:673–6.
67. Grive KJ, Hu Y, Shu E, Grimson A, Elemento O, Grenier JK, et al. Dynamic transcriptome profiles within spermatogonial and spermatocyte populations during postnatal testis maturation revealed by single-cell sequencing. PLoS Genet 2019;15:e1007810.

Supplementary Material: This article contains supplementary material (https://doi.org/10.1515/med-2025-1344).